Electronic Supplementary Material (ESI) for Journal of Materials Chemistry C.
This journal is © The Royal Society of Chemistry 2018

Supplementary Information

Insight into Chirality on Molecular Stacking for Tunable Ultralong Organic Phosphorescence

Chaoqun Ma,[a,†] Huili Ma,[a,†] Kun Ling,[a] Ruilin Zheng,[b] Mingxing Gu,[a] Lulu Song,[a]

Zhongfu An,[,a] Huifang Shi,*[,a] and Wei Huang*[a,c]*

[a.]Key Laboratory of Flexible Electronics (KLOFE) & Institute of Advanced Materials (IAM) Nanjing Tech University (NanjingTech), 30 South Puzhu Road, Nanjing 211800, China.

[b.]College of Electronic and Optical Engineering, Nanjing University of Posts & Telecommunications, 9 Wenyuan Road, Nanjing 210023, China.

[c.]Shaanxi Institute of Flexible Electronics (SIFE) Northwestern Polytechnical University (NPU), 127 West Youyi Road, Xi'an 710072, China.

*E-mail: iamzfan@njtech.edu.cn; iamhfshi@njtech.edu.cn;

iamwhuang@njtech.edu.cn

[†] Chaoqun Ma, Huili Ma contributed equally.

Experimental Section

Reagents and materials: 2,4,6-Trichloro-1,3,5-triazine was purchased from Energy Chemical. 9*H*-carbazole was purchased from Alfachem Co., Ltd. (Zhengzhou). 1-Phenylethan-1-ol and n-butyllithium were purchased from J&K Chemical. (S)-1-Phenylethan-1-ol was purchased from LookChem. Those materials were used as received without further purification. Tetrahydrofuran (THF) was dried by distillation with sodium as desiccant and benzophenone as chromogenic reagent.

Measurements: Nuclear magnetic resonance (^{1}H NMR and ^{13}C NMR) spectra were determined on a Bruker Ultra Shield plus 400 MHz spectrometer in $CDCl_3$. Tetramethylsilane (TMS) was used as the internal standard of chemical shifts. And resonance patterns were signed with the notations s (singlet), d (double), t (triplet), q (quartet), and m (multiplet). Molecular mass was measured by an autoflex speed MALDI- TOF. Gel filtration chromatography was performed using a BEH C18 column conjugated to an ACQUITY UPLC water HPLC system. Before running, each sample was purified via 0.22 μm filter to remove any aggregates. The flow rate was fixed at 0.3 mL/min, the injection volume was 2 μL and each sample run for 6 min. 100% of methanol was used as the mobile phase. Thermogravimetric analyses (TGA) of samples were conducted by Mettler TGA2. Samples were held in a platinum pan under nitrogen atmosphere. A 10 K min^{-1} ramp rate was used. Ultraviolet-visible absorption spectra were obtained using a Shimadzu UV-1750. Steady-state fluorescence and phosphorescence spectra were recorded on F-4600 fluorescence spectrophotometer. The phosphorescence spectra were collected with a delay time of 5 ms. The phosphorescence lifetimes were measured using Edinburgh FLSP920 fluorescence spectrophotometer equipped with a nanosecond LED lamp (nF920) and

a microsecond flash-lamp (μF900). Photoluminescence quantum yields were measured by Hamamatsu Absolute PL Quantum Yield Spectrometer C11347. The photographs were taken using a Cannon EOS 700D camera with a hand-held 365 nm ultraviolet lamp switched on and off. The measurements at 77 K were achieved in the liquid nitrogen. High performance liquid chromatography was applied to check their purities before photophysical measurement.

Single crystal X-Ray Diffraction: X-ray crystallography was determined using a Bruker SMART APEX-II CCD diffractometer with graphite monochromated Mo-Kα radiation. Cambridge Crystallographic Data Centre (CCDC) 1817670 and 1817671 contain the supplementary crystallographic data for this paper. These data can be acquired free of charge from The Cambridge Crystallographic Data Centre via www.ccdc.cam.ac.uk/data_request/cif.

Computational Methods: The computational models were built from the crystal structure shown in Chart 1. The quantum mechanics/molecular mechanics (QM/MM) theory with two-layer ONIOM method was implemented to deal with the electronic structures in crystal, where the central molecule is chosen as the active QM part and set as the high layer, while the surrounding ones are chosen as the MM part and defined as the low layer. The universal force field (UFF) was used for the MM part, and the molecules of MM part were frozen during the QM/MM geometry optimizations. The geometries and the vibrational frequencies of the ground state (S_0) and the lowest triplet states (T_1) were evaluated at (U)B3LYP/6-31G(d) level, while the excitation energies were calculated by using TD-DFT for the excited singlet and triplet

states. The above results were calculated by Gaussian 09 package.[1] At the same level, the spin-orbit coupling (SOC) of $T_1 \rightarrow S_0$ was given by Beijing Density Function (BDF) program.[2-4]

The phosphorescence lifetime τ_{p} of $T_1 \rightarrow S_0$ is determined by the radiative rate k_{p} and non-radiative decay rate k_{nr}, and defined as follows:[5,6]

$$\tau_{\mathrm{p}} = 1/(k_{\mathrm{p}} + k_{\mathrm{nr}})$$

$$k_{\mathrm{p}} = \frac{E^2 f}{1.499\ \mathrm{cm}^2 \cdot \mathrm{s}}$$

$k_{\mathrm{nr}} \propto \frac{2\pi}{h} |\langle \psi_1^3 | H_{\mathrm{SO}} | \psi_0^1 \rangle|^2 exp(-E/\lambda)$, where ψ_0^1 and ψ_1^3 are the electronic wavefunction of S_0 and T_1, respectively; H_{SO} is the spin-orbit coupling operator between T_1 and S_0; E and f are the excitation energy and oscillator strengthen of $T_1 \rightarrow S_0$; λ is the reorganization energy. It is evidently the reduction of spin-orbit coupling and reorganization energy facilitates the prolonging of phosphorescence lifetime.

Scheme S1. Synthetic routes of SPCzT and PCzT molecules.

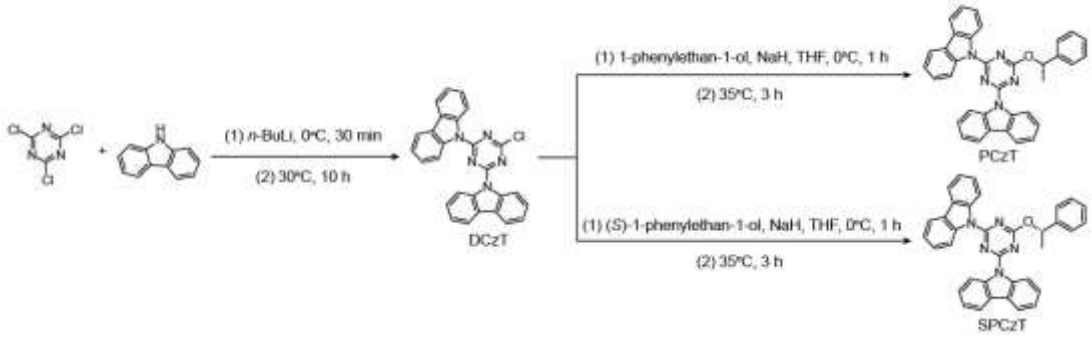

Synthesis of SPCzT and PCzT compounds

Synthesis of 9,9'-(6-chloro-1,3,5-triazine-2,4-diyl)bis(9H-carbazole) (DCzT): Compound DCzT was synthesized according to the literature.[7] ^{1}H NMR (400 MHz, $CDCl_3$): δ 8.82 (d, 4H), 7.97 (d, 4H), 7.39-7.56 (m, 8H).

Synthesis of SPCzT: Mixed Sodium (0.023 g, 1 mmol) and (S)-1-phenylethan-1-ol (1 mL, 0.81 mmol) were added into a 10 mL round-bottom flask with tetrahydrofuran (0.5 mL) and stirred

at room temperature for 2 h to form sodium salt. The sodium salt solution was added into round-bottom flask charged with DCzT (0.29 g, 0.818 mmol) solution at 35°C. After stirring at 35°C overnight, tetrahydrofuran was removed by rotary evaporation. Then the product was further extracted with CH_2Cl_2 and water for three times. After CH_2Cl_2 was removed by rotary evaporation, the target compound was purified by flash column chromatography to give white powder with a high yield of 22.4%. ^{1}H NMR (400 MHz, $CDCl_3$): δ 8.81 (d, 4H), 8.08 - 8.03 (m, 4H), 7.62-7.57 (m, 2H), 7.48-7.32 (m, 11H), 6.44 (q, 1H), 1.89 (d, 3H). ^{13}C NMR (100 MHz, $CDCl_3$): δ 170.87, 165.45, 142.07, 138.81, 128.76, 127.96, 126.94, 126.42, 125.60, 123.33, 119.63, 117.58, 76.41, 23.79. MALDI-TOF MS (m/z): calcd for $C_{35}H_{25}N_5O$, 531.62. Found: 530.82. Element analysis (CHNS mode): calcd for $C_{35}H_{25}N_5O$, N (13.17%), C (79.08%), H (4.74%). Measured: N (13.17%), C (79.09%), H (4.63%).

Synthesis of PCzT: Following the same synthetic procedure of SPCzT, 1-phenylethan-1-ol (racemization, 1 mL, 0.818 mmol), sodium (0.023 g, 1 mmol) and DCzT (0.29 g, 0.818 mmol) produced white powder with a yield of 18.4%. ^{1}H NMR (400 MHz, $CDCl_3$): δ 8.81 (d, 4H), 8.01-8.08 (m, 4H), 7.61 (d, 2H), 7.50-7.32 (m, 11H), 6.43 (q, 1H), 1.89 (d, 3H). ^{13}C NMR (100 MHz, $CDCl_3$): δ 170.86, 165.45, 142.08, 138.81, 128.77, 127.97, 126.94, 126.42, 125.60, 123.33, 119.63, 117.58, 76.41, 23.81. MALDI-TOF MS (m/z): calcd for $C_{35}H_{25}N_5O$, 531.62. Found: 530.775. Element analysis (CHNS mode): calcd for $C_{35}H_{25}N_5O$, N (13.17%), C (79.08%), H (4.74%). Measured: N (13.1%), C (78.85%), H (4.66%).

The preparation of crystals: Prepared powder of SPCzT (10 mg) were resolved in chloroform solvent (1 mL) and let stand until no solid can be observed by naked eyes. After this, petroleum ether (1-2 mL) were slowly added into above solution as a poor solvent. Then, the mixture

should be keeps in an undisturbed environment about 25 ^{o}C for two days for crystal formation and resulting in octahedral bulk crystal. The rodlike PCzT crystals were cultivated in the same condition as SPCzT.

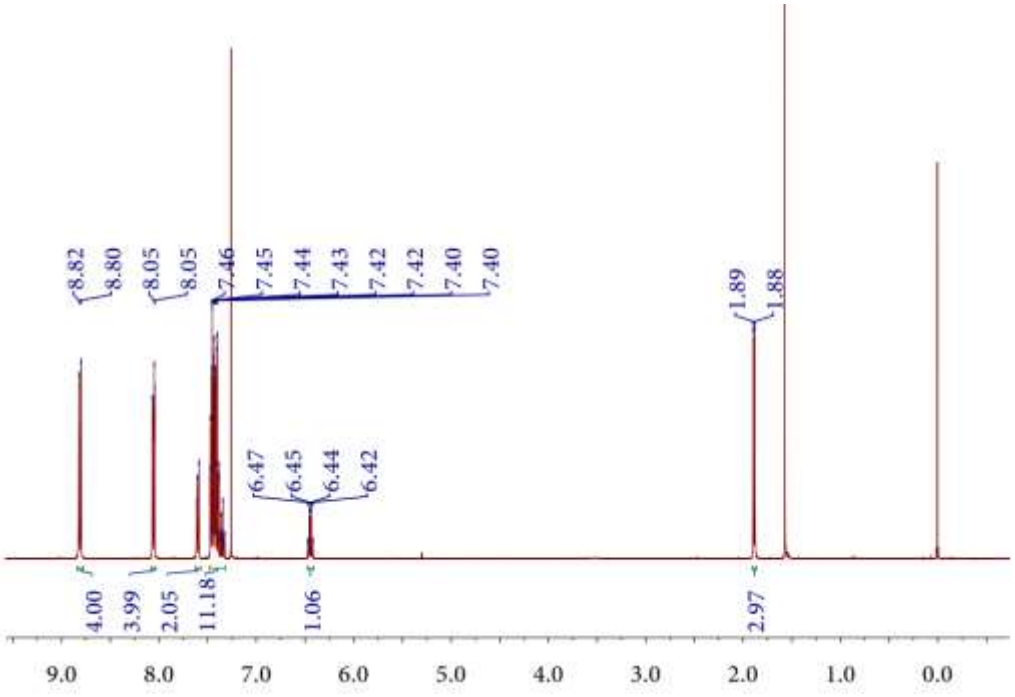

Figure S1. ^{1}H NMR spectrum of SPCzT in $CDCl_3$.

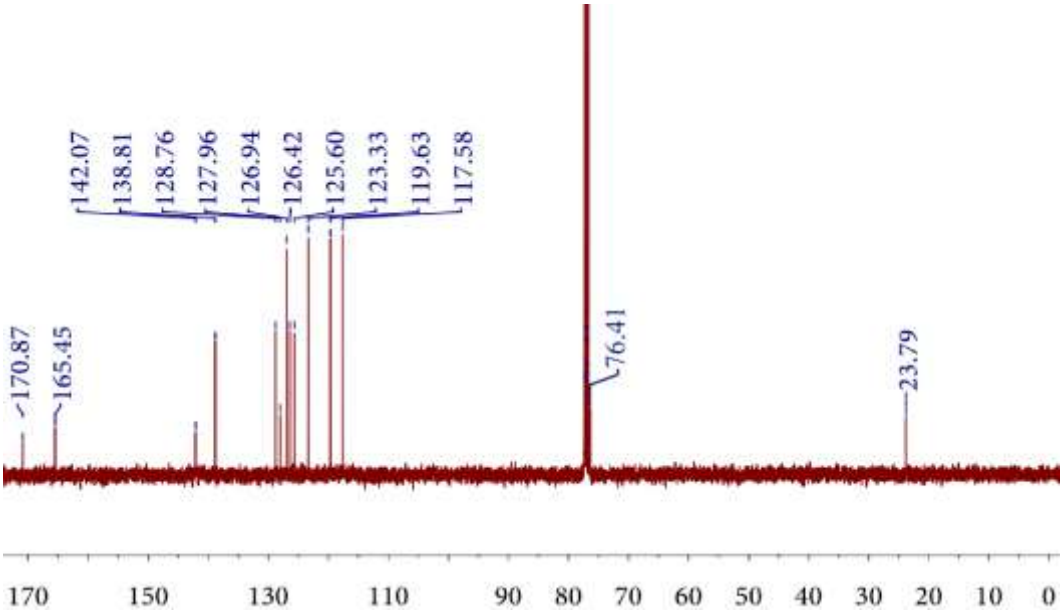

Figure S2. ^{13}C NMR spectrum of SPCzT in $CDCl_3$.

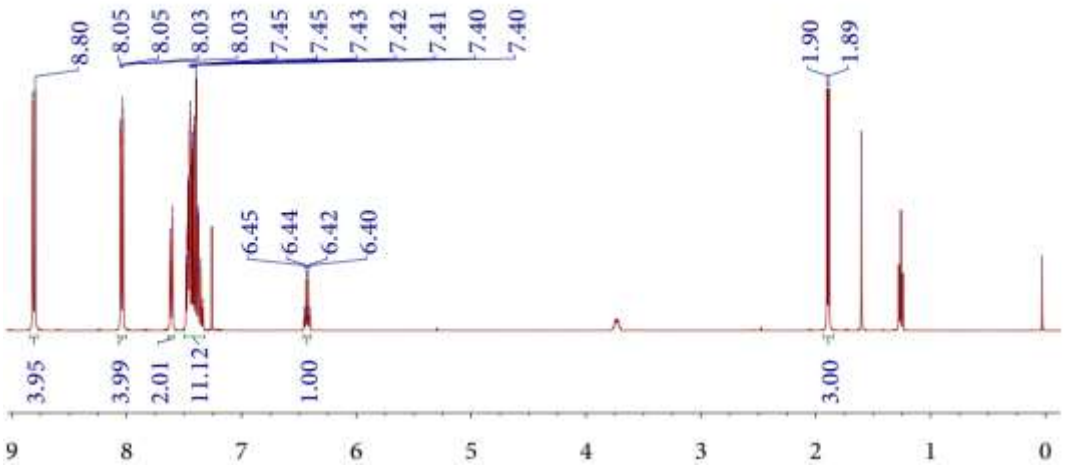

Figure S3. ^{1}H NMR spectrum of PCzT in $CDCl_3$.

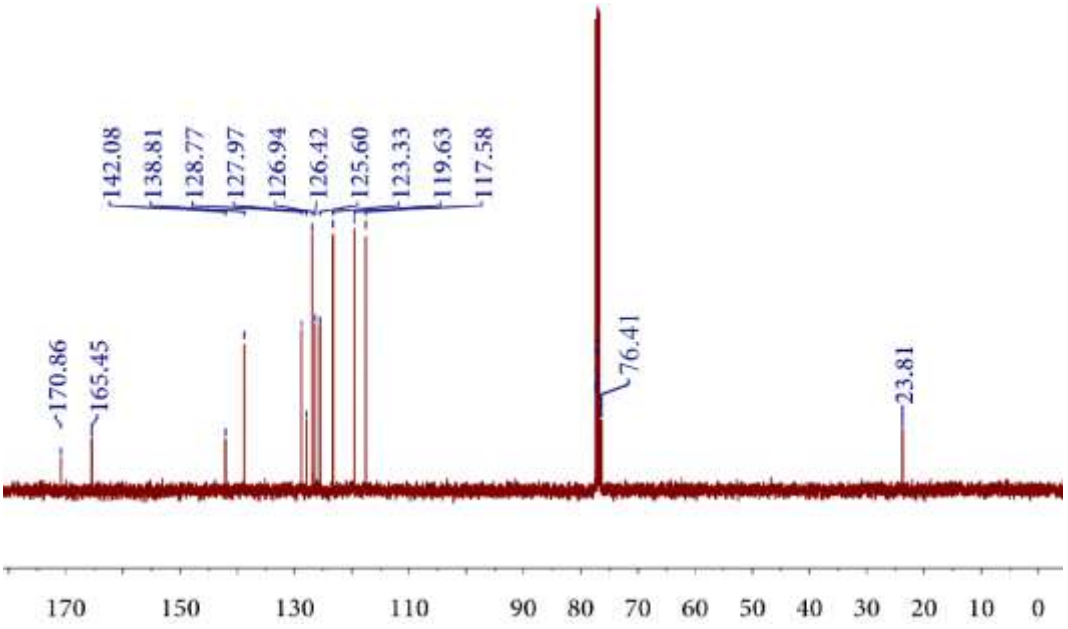

Figure S4. ^{13}C NMR spectrum of PCzT compound in $CDCl_3$.

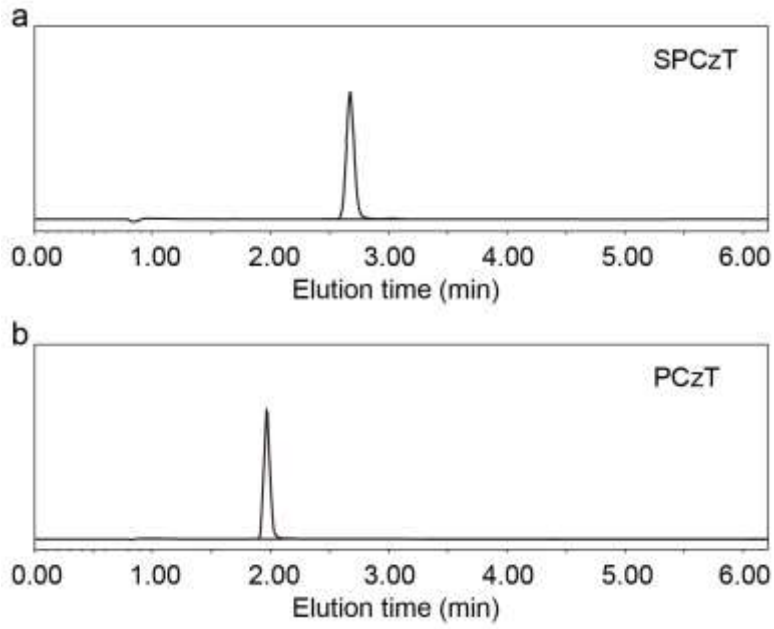

Figure S5. High-performance liquid chromatogram spectra of SPCzT and PCzT in methanol solution.

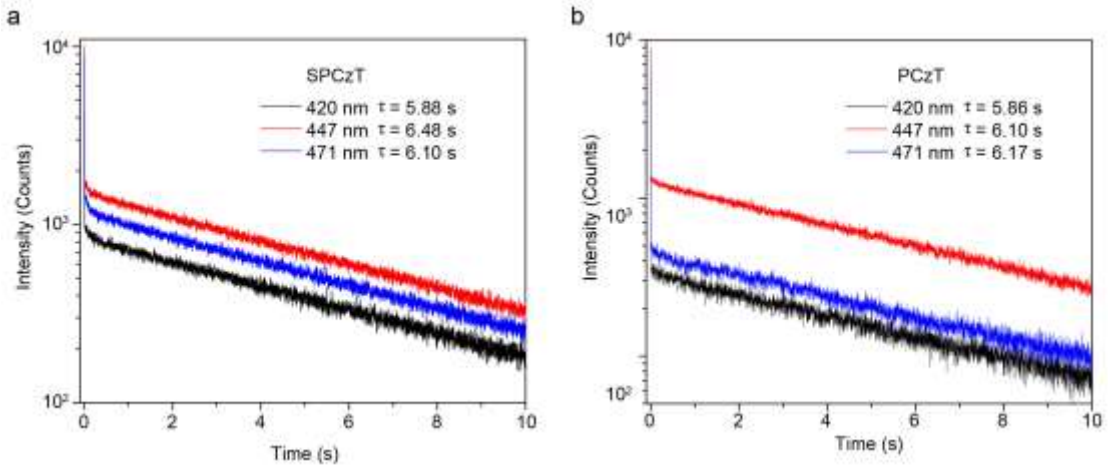

Figure S6. Time-resolved decay curves of the emission bands at 420, 447 and 471 nm for (a) SPCzT and (b) PCzT in dilute dimethyl tetrahydrofuran solution at 77 K, respectively.

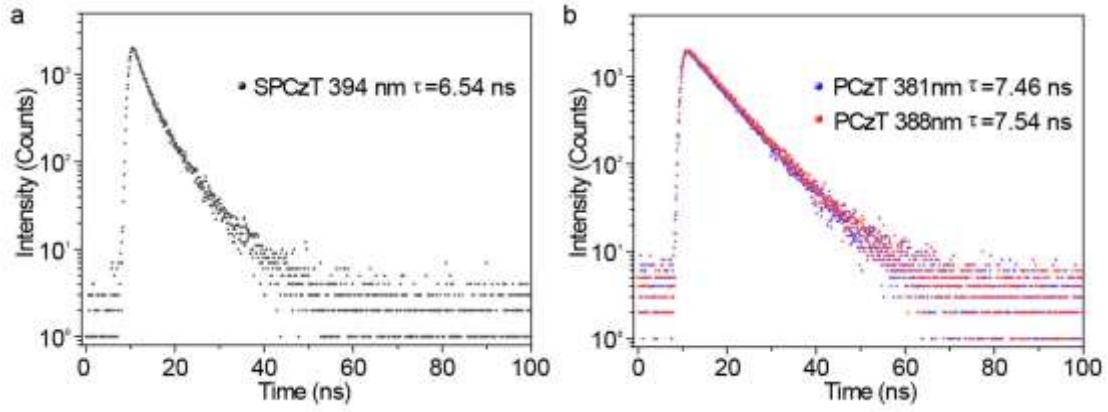

Figure S7. Time-resolved decay curves of the emission bands at (a) 394 nm for SPCzT and (b) 381 nm, 388 nm for PCzT in crystal state under ambient conditions, respectively.

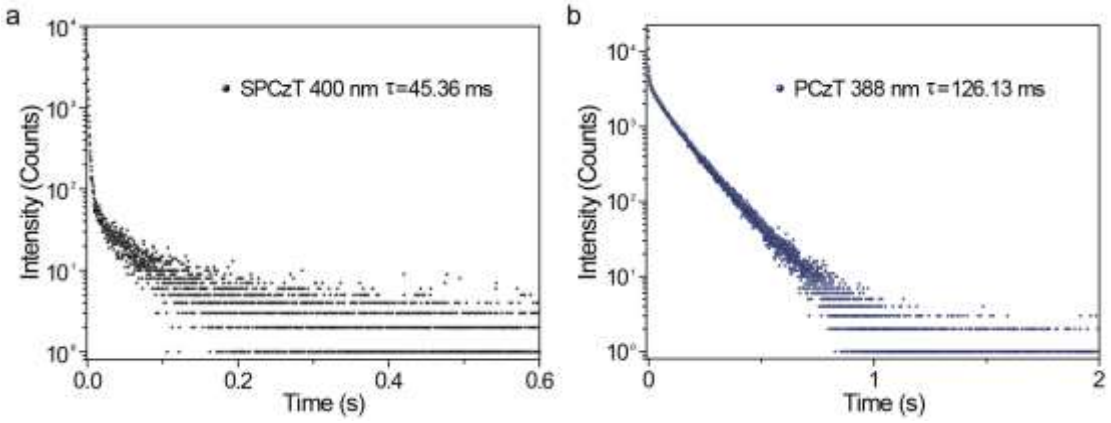

Figure S8. Time-resolved decay curves of the emission bands at (a) 400 nm for SPCzT and (b) 388 nm for PCzT in crystalline state under ambient conditions, respectively.

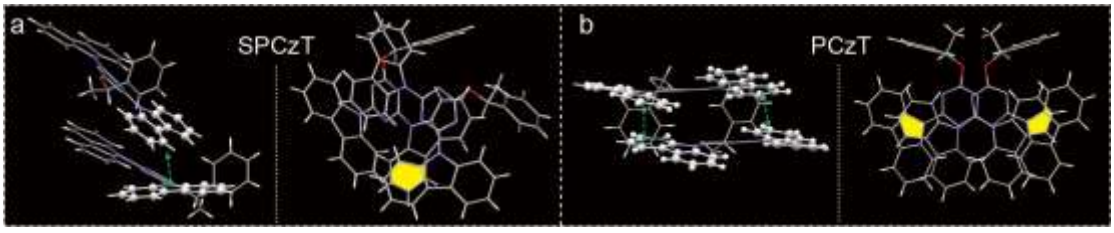

Figure S9. Molecular packing of the dimers of (a) SPCzT and (b) PCzT crystals, respectively. Yellow areas show the π-π overlap of carbazoles.

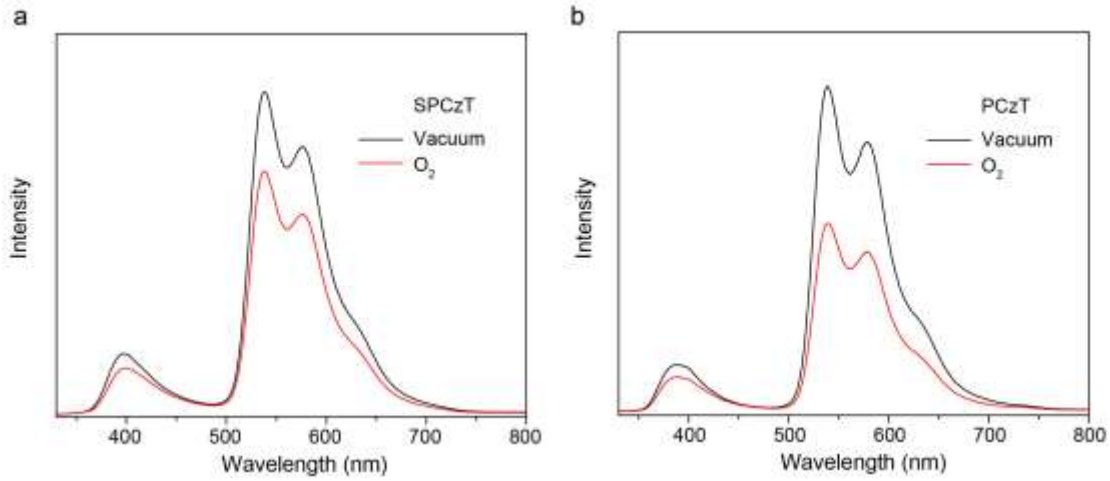

Figure S10. Phosphorescence spectra of (a) SPCzT and (b) PCzT crystals in vacuum (black line) and O_2 (red line), respectively.

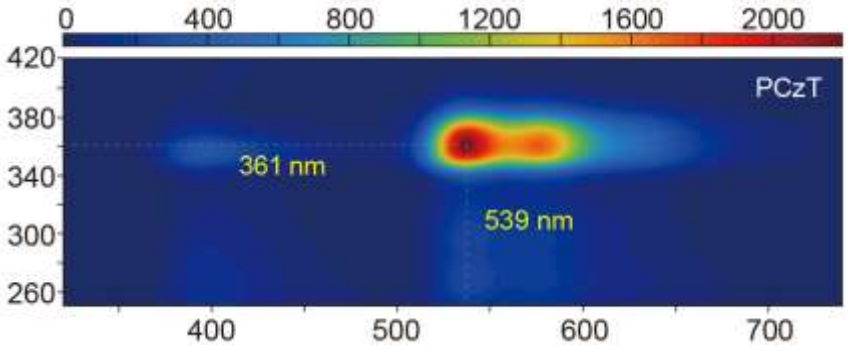

Figure S11. Excitation-phosphorescence mapping of PCzT crystal under ambient conditions.

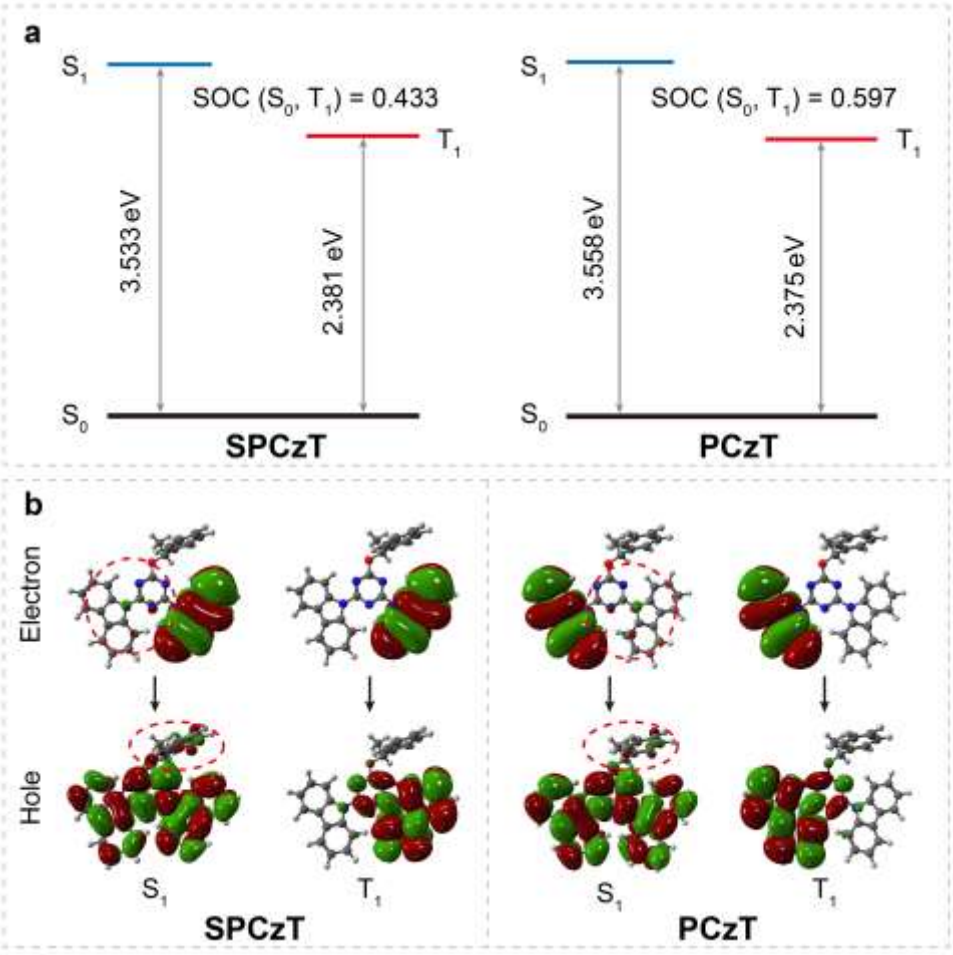

Figure S12. (a) Calculated excitation energies and SOC as well as (b) Natural transition orbitals (NTOs) for the lowest excited singlet and triplet states of SPCzT and PCzT molecules in crystal.

Both SPCzT and PCzT showed the same fluorescence with broad profiles in solution, implying a charge transfer (CT) transition. While the same phosphorescence with vibrational peaks was also observed in solution at 77 K, indicating a local excitation (LE) transition. It is known that the charge transfer transition is sensitive to the molecular environment, whereas the local transition is dull.[8] Upon crystallization, the fluorescence emission displayed different vibrational profile with the same emission position, whereas the phosphorescence emission was the same with two peaks of 539 and 580 nm. Namely, the different molecular packing

environment in SPCzT and PCzT was responsible to the different fluorescence spectra. To further explore the difference in fluorescence emission, TDDFT calculations were performed in Figure S12 in Supporting Information. It is found that the excitation energies of S_1 and T_1 in SPCzT and PCzT are almost the same, resulting in the same emission position in fluorescence and phosphorescence. In addition, S_1 of both SPCzT and PCzT are the admixture of LE and CT transition and shows a slight difference in the natural transition orbitals, which contributes to the difference in fluorescence spectra. Whereas the T_1 showed the same LE transition, thus the difference in phosphorescence of SPCzT and PCzT is tiny.

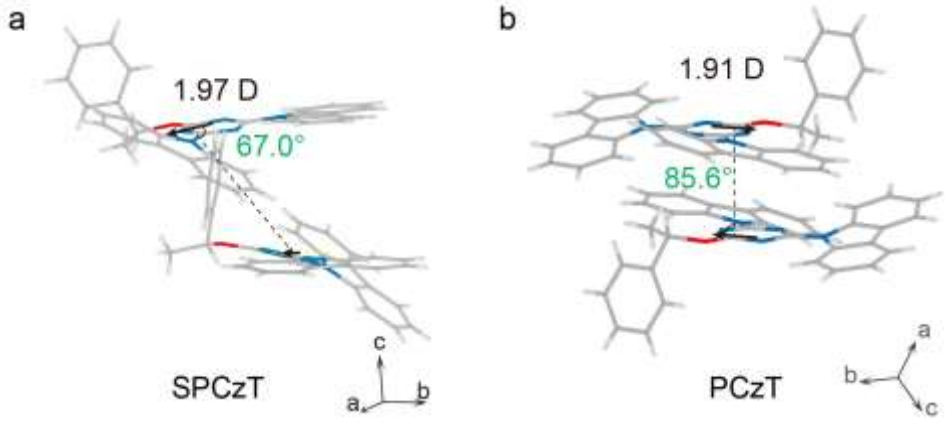

Figure S13. Dimers with H-aggregation of (a) SPCzT and (b) PCzT in single crystal, respectively. Their transition dipole moments and measured angles between transition dipoles and interconnected axis are marked.

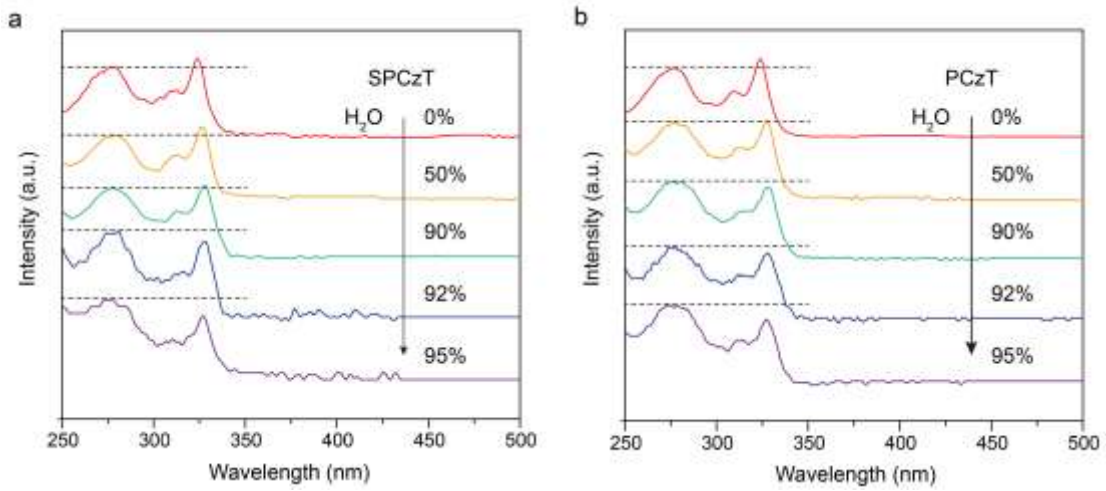

Figure S14. The absorption spectra of (a) SPCzT and (b) PCzT (1×10^{-5} M) with increasing water content from 0 vol% to 95 vol % in methanol.

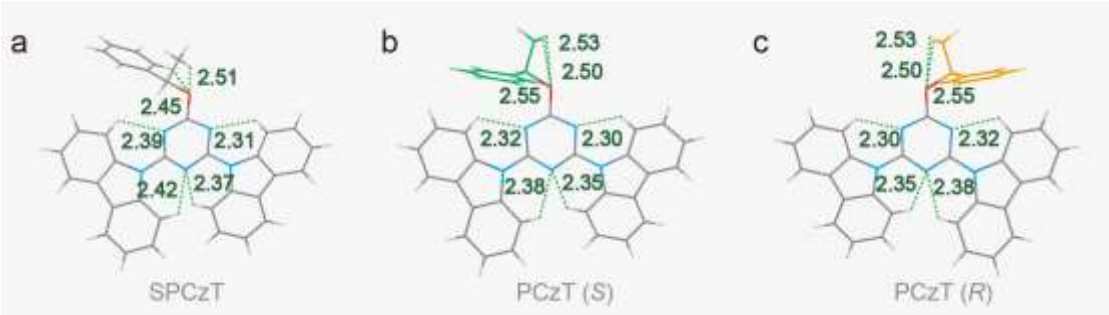

Figure S15. Intramolecular interactions of (a) SPCzT and (b) PCzT in single crystal, respectively.

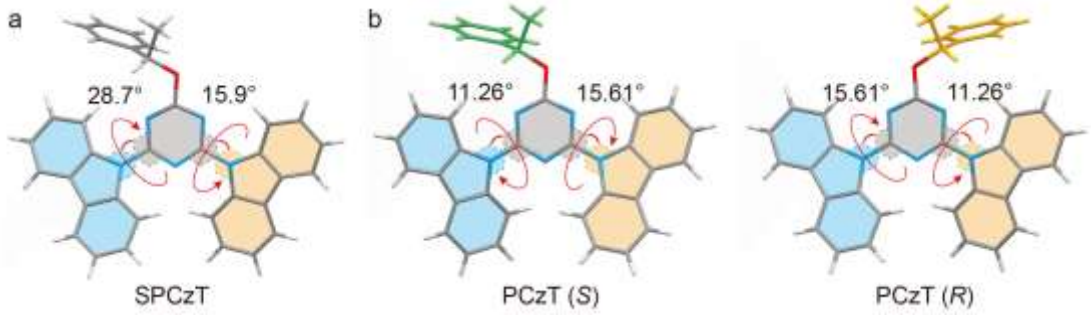

Figure S16. Dihedral angles between the carbazole groups and the triazine core of (a) SPCzT and (b) PCzT in crystal state, respectively.

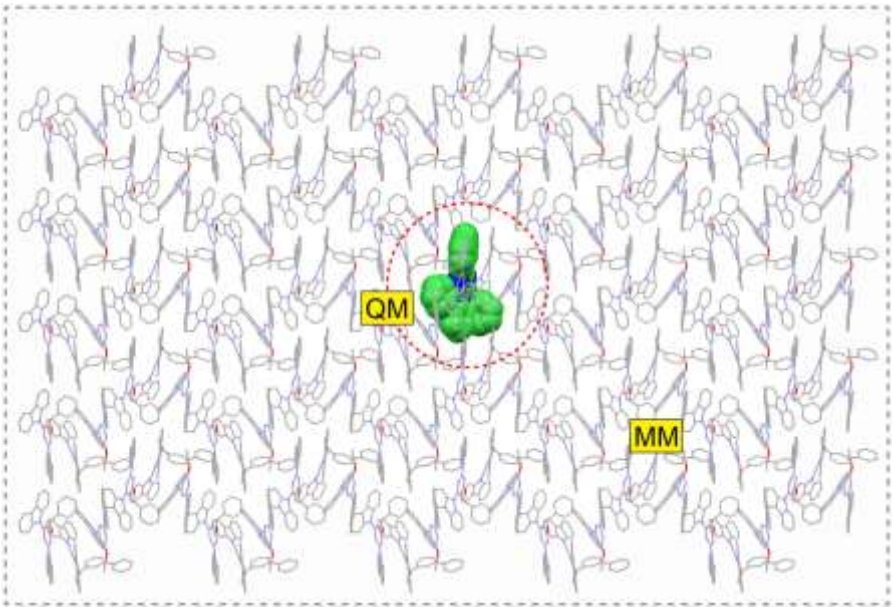

Figure S17. QM/MM model of SPCzT. The central green molecule circled by red dotted line is embeded in the whole molecular packing (5×5×5) as the QM model of SPCzT, which modulates solid environment. Note that a central QM molecule for the higher layer and the remaining MM molecules for the lower layer.

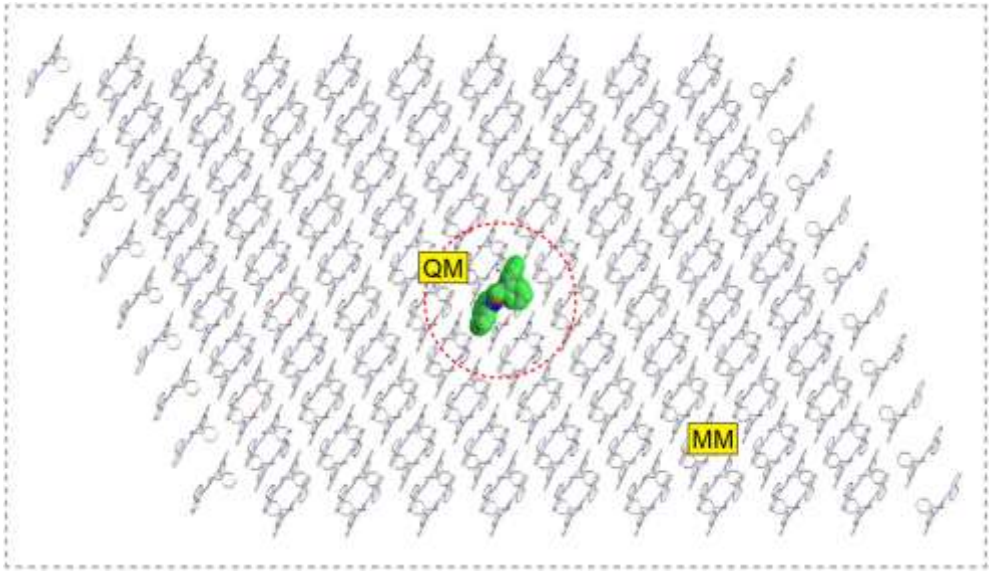

Figure S18. QM/MM model of PCzT(S). The central green molecule circled by red dotted line is embeded in the whole molecular packing (5×5×5) as the QM model of PCzT, which modulates solid environment. Note that a central QM molecule for the higher layer and the remaining MM molecules for the lower layer.

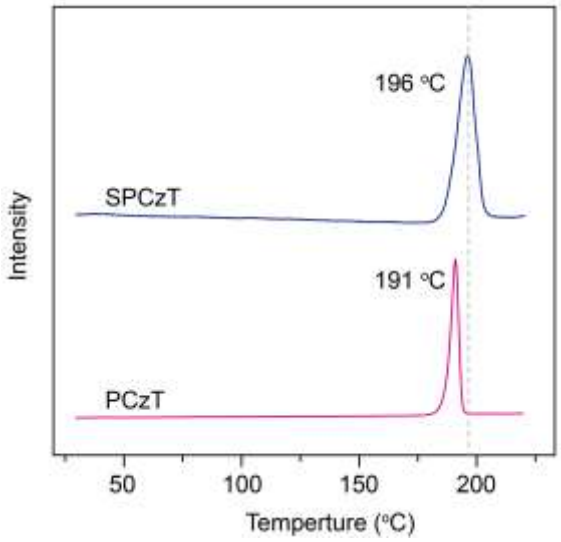

Figure S19. Thermogravimetric analysis (TGA) curves of SPCzT and PCzT in crystal state, respectively.

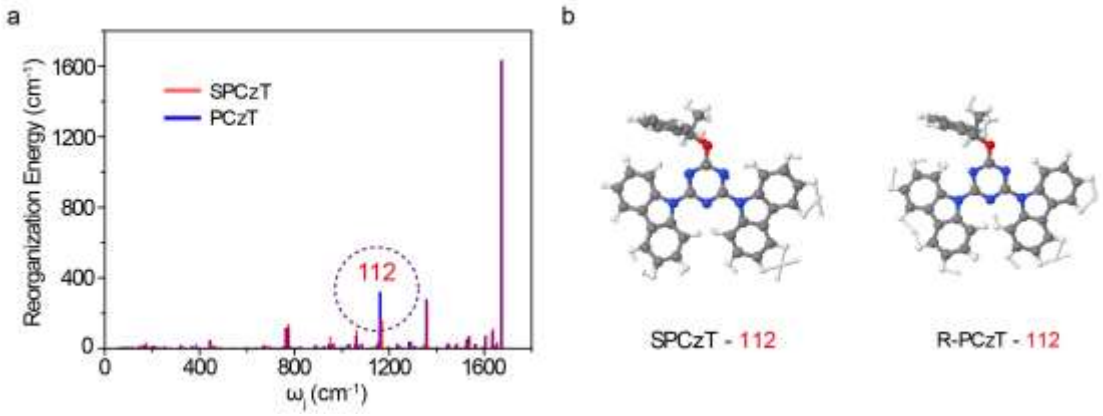

Figure S20. (a) Calculated reorganization energy (λ_j) versus ω_j of SPCzT and PCzT in crystal state, respectively. (b) Selected normal modes of SPCzT and PCzT with different reorganization energy.

Table S1 Lifetimes of crystalline SPCzT and PCzT at different emission wavelengths under ambient conditions

Compound	Wavelength (nm)	Fluorescence				Ultralong luminescence					
		τ_1 (ns)	A_1 (%)	τ_2 (ns)	A_2 (%)	τ_1 (ms)	A_1 (%)	τ_2 (ms)	A_2 (%)	τ_3 (ms)	A_3 (%)
SPCzT	394	6.54	47.26	2.41	52.74	-	-	-	-	-	-
	400	-	-	-	-	45.36	32.04	2.72	25.84	0.68	43.72
	539					419.8	83.12	25.31	16.88	-	-
	580					395.9	80.16	28.58	19.84	-	-
PCzT	381	7.46	100	-	-	-	-	-	-	-	-
	397	7.54	100	-	-	-	-	-	-	-	-
	388	-	-	-	-	126.13	79.27	44.83	17.5	1.19	3.23
	539	-	-	-	-	229.04	100	-	-	-	-
	580	-	-	-	-	215.41	100	-	-	-	-

Table S2 Photoluminescence quantum efficiencies of crystalline SPCzT and PCzT under ambient conditions

Compound	Fluorescence	Phosphorescence
SPCzT	30.42%	0.58%
PCzT	13.89%	0.1%

Table S3 Molecular interactions in crystalline SPCzT and PCzT

Types of Interactions		SPCzT (Å)	PCzT (Å)
Intramolecular interactions	O···H	2.449, 2.513	2.500, 2.534, 2.550
	N···H	2.422, 2.372, 2.309, 2.395	2.324, 2.378, 2.351, 2.303
Intermolecular interactions	π-H···C	2.819, 2.817	-
	C-H···π	2.870, 2.877, 3.374	-
	π-H···O	-	2.662
	π···π	3.366, 3.369, 3.357	3.386, 3.327, 3.293
	π-H···π	2.745, 2.751, 2.865, 2.855, 2.893, 2.857, 2.850, 2.887	2.769
	π-H···H-π	2.357, 2.348	2.289

Table S4. Dynamic photophysical parameters of the ultralong organic phosphorescent molecules SPCzT and PCzT.

Compound	Fluorescence	Phosphorescence			
	τ_{fluo} (ns)	τ_{Phos} (ms)	φ (%)	k_r^{Phos} (s^{-1})[a]	k_{nr}^{Phos} (s^{-1})[b]
SPCzT	6.54	419.8	0.58	1.38×10^{-2}	2.37
PCzT	7.54	229.04	0.1	4.37×10^{-2}	4.36

[a] $k_r^{Phos} = \varphi_{Phos}/\tau_{Fluo}$; [b] $k_{nr}^{Phos} = (1 - \varphi_{Phos})/\tau_{Phos}$.

References

(1) M. J. Frisch, G. W. Trucks, H. B. Schlegel, G. E. Scuseria, M. A. Robb, J. R. Cheeseman, G. Scalmani, V. Barone, B. Mennucci, G. A. Petersson, H. Nakatsuji, M. Caricato, X. Li, H. P. Hratchian, A. F. Izmaylov, J. Bloino, G. Zheng, J. L. Sonnenberg, M. Hada, M. Ehara, K. Toyota, R. Fukuda, J. Hasegawa, M. Ishida, T. Nakajima, Y. Honda, O. Kitao, H. Nakai, T. Vreven, J. A. Montgomery Jr., J. E. Peralta, F. Ogliaro, M. J. Bearpark, J. Heyd, E. N. Brothers, K. N. Kudin, V. N. Staroverov, R. Kobayashi, J. Normand, K. Raghavachari, A. P. Rendell, J. C. Burant, S. S. Iyengar, J. Tomasi, M. Cossi, N. Rega, N. J. Millam, M. Klene, J. E. Knox, J. B. Cross, V. Bakken, C. Adamo, J. Jaramillo, R. Gomperts, R. E. Stratmann, O. Yazyev, A. J. Austin, R. Cammi, C. Pomelli, J. W. Ochterski, R. L. Martin, K. Morokuma, V. G. Zakrzewski, G. A. Voth, P. Salvador, J. J. Dannenberg, S. Dapprich, A. D. Daniels, Farkas, J. B. Foresman, J. V. Ortiz, J. Cioslowski, D. J. Fox, Gaussian 09. Revision B.01., Gaussian, Inc. Wallingford, con, USA, 2009.

(2) W. Liu, F. Wang, D. Dai, L. Li, M. Dolg, *Theor. Chem. Acc.,* 1997, **96**, 75.

(3) W. Liu, G. Hong, L. Li, *J. Theor. Comput. Chem.,* 2003, **2**, 257.

(4) K. Hirao, Y. Ishikawa, Recent Advances in Computational Chemistry, World Scientific, Singapore, 2004.

(5) W. J. Zhao, Z. K. He, J. W. Y. Lam, Q. Peng, H. L. Ma, Z. G. Shuai, G. X. Bai, J. H. Hao, B. Z. Tang, *Chem.,* 2016, **1**, 592.

(6) H. L. Ma, W. Shi, J. J. Ren, W. Q. Li, Q. Peng, Z. G. Shuai, *J. Phys. Chem. Lett.,* 2016, **7**, 2893.

(7) Z. F. An, R. F. Chen, J. Yin, G. H. Xie, H. F. Shi, T. Tsuboi, W. Huang, *Chem.-Eur. J.,* 2011, **17**, 10871.

(8) M. K. Etherington, F. Franchello, J. Gibson, T. Northey, J. Santos3 J. S. Ward, H. F. Higginbotham, P. Data, A. Kurowska, P. L. D. Santos, D. R. Graves, A. S. Batsanov, F. B. Dias, M. R. Bryce, T. J. Penfold, A. P. Monkman, *Nat. Commun.,* 2017, **8**, 14987.